Veröffentlichung

Im Rahmen des SFB 880. www.sfb-880.tu-bs.de

Autoren:	T. Beutel, M. Leester-Schädel, S. Büttgenbach
Titel:	**Design and evaluation process of a robust pressure sensor for measurements in boundary layers of liquid fluids**
Journal, Seite, Verlag:	Microsystem Technologies (ISSN 0946-7076), Volume 18, Issue 7 (2012), pp. 893-903, Springer Verlag
Konferenz, Ort:	
Jahr:	2011
Internet-Link (Doi-Nr.):	http://dx.doi.org/10.1007/s00542-011-1404-x

The original publication is available at www.springerlink.com

Microsyst Technol
DOI 10.1007/s00542-011-1404-x

TECHNICAL PAPER

Design and evaluation process of a robust pressure sensor for measurements in boundary layers of liquid fluids

T. Beutel · M. Leester-Schädel · S. Büttgenbach

Received: 19 July 2011 / Accepted: 9 December 2011

Abstract In this work, the latest results of the design, fabrication and characterization of a new MEMS piezoresistive pressure sensor are presented. Significant changes in the layout as well as in the micro-fabrication process have been made, e.g. anodic bonding of a glass cover on the backside. The sensor has been developed in order to meet the special requirements of measurements in fluid mechanics, particularly with regard to the non-intrusive nature of the sensor. The sensor development, starting with the simulation of mechanical stresses within the diaphragm resulting from a pressure of up to 4 bar is described. These calculations have lead to an optimized placement of the piezoresistors in order to achieve a maximum sensitivity. Important parameters including sensitivity, resonance frequency and maximum load are described precisely. The experiments and the initial results, e.g. its linearity and its dynamic capability are demonstrated.

1 Introduction

Due to the ever increasing costs of energy, as well as aspects of environmental protection, ever more efficient products must be developed. In the aeronautical industry it is therefore necessary to continually investigate new concepts to reduce the fuel consumption and noise emission of civil aircraft. It is additionally important that airplane noise emissions during takeoff are extremely high and no longer accepted by the population. New aircraft models have therefore to be evaluated already in the development phase. The accelerated requirements of customers make these analyses even more important.

In a new approach to achieve high lift a Coanda flap is used. By controlling suction and blow out of compressed air at discrete places along the wing shape, the drag is expected to be reduced significantly. The exhausted air is used to accelerate the near wall flow velocity above the Coanda flap in order to maintain a laminar flow and generate a high lift coefficient C_L. Current results of numerical investigations show that pulsed exhaust can produce similar performance to continuous flow with even less energy consumption, which is essential for a high over-all performance including all subsystems. With new piezoelectric actuators, which make changes to their length under high voltage excitation, it is possible to change the contour of wing sections. An oscillating lip enables pulsed blowing at the necessary frequency, by changing the height of the blowing slot.

This concept requires the ability to measure the state of the flow at high frequency and to be able to control it in real time. Novel sensors are therefore required to enable time critical measurements of the flow conditions. These requirements have lead to the development of new sensor modules which are able to non-intrusively detect the state of the flow. Due to the reasons described, the sensor modules have to measure two parameters. In addition to the pressure value, information about the wall shear stress is necessary to characterize the flow more exactly. For this reason a hot-film sensor will be integrated into the same chip, which has no significant impact on the overall shape of the sensor modules. In this work the pressure sensor is described, based on a membrane structure and piezoresistive effect.

T. Beutel (✉) · M. Leester-Schädel · S. Büttgenbach
Institute for Microtechnology (IMT), Technische Universität Braunschweig, Alte Salzdahlumer Straße 203, 38124 Braunschweig, Germany
e-mail: T.Beutel@TU-Braunschweig.de

Published online: 24 December 2011

Due to economic and technological reasons, it is advisable to use carbon fibre laminate as the wing's skin and it has been shown (Beutel et al. 2010a, b) that it is feasible to implement micro-fabricated sensors (AeroMEMS) flush to the fluid. In this manuscript we describe the design and fabrication processes of second generation pressure sensors. All improvements are described precisely. Additionally, the initial measurement results are presented and discussed in the next subsection. Finally an outlook is provided.

2 Sensor concept

In this section the reasons for a new pressure sensor concept are explained. The boundary conditions set by the fabrication, the environmental conditions, the embedding process into fibre material and the measurement purposes are described. At the end of each subsection the consequences for the sensor concept are summarized. This chapter leads to the design rules on which the sensor is based.

2.1 Basic geometry and limitations

This new approach to efficient active high lift requires the fabrication of a novel sensor module. The main goal is to enable pressure and wall shear stress measurements at frequencies of at least 1 kHz without disturbing the flow itself. Consequently the mounting of the sensor modules and actuators have to be flush to the wall. Therefore, it is a perfect solution to embed both into fibre composite material. This material is stiff enough to support the sensors and yet is flexible enough to change its contour due to the actuation. Figure 1 shows the concept of the actuated lip in detail. The actuation enables high frequent changes of the slot height h. Because of a constant mass flow of pressurized air $\dot{m}$, the velocity V changes. This concept is expected to influence the flow above the Coanda flap in the desired manner.

Because of the high demands on measuring frequency and accuracy, the first measurements will be performed in a water tunnel to reduce the control complexity of the system. Due to the high density of water, the needed system frequency is ten times lower than in air. This simplifies the first steps in the experimental phase. In contrast, measuring in water with the micro-fabricated sensor modules will be a challenge. The combination of pressure sensor and a hot-wire sensor is considered to be a promising development mentioned in many studies (Ebefors et al. 1998; Schiffer et al. 2005; Berns et al. 2008).

The pressure coefficient C_p over the entire airfoil was obtained from the project partners who conducted numerical experiments of the aerodynamic section. The maximum and minimum loads on the pressure sensor are therefore able to be calculated.

In Fig. 2 the principle of mechanical stress measurement in the sensor is illustrated. Figure 2a shows a sectional

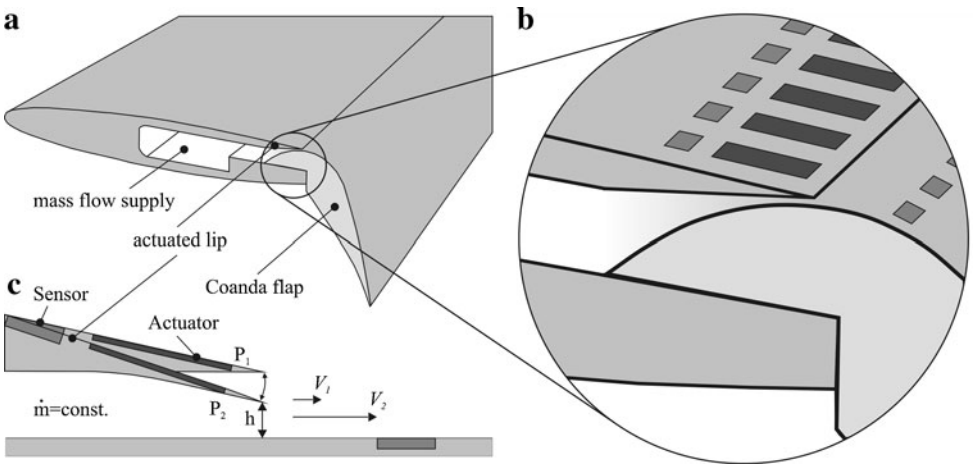

Fig. 1 **a** Scheme of the wing chord with a detailed drawing **b** of the sensor and actuator system placed over a Coanda flap for active high lift. Part **c** explains how the actuator moves the lip between the positions P_1 and P_2, resulting in the velocity V_1 and V_2, respectively

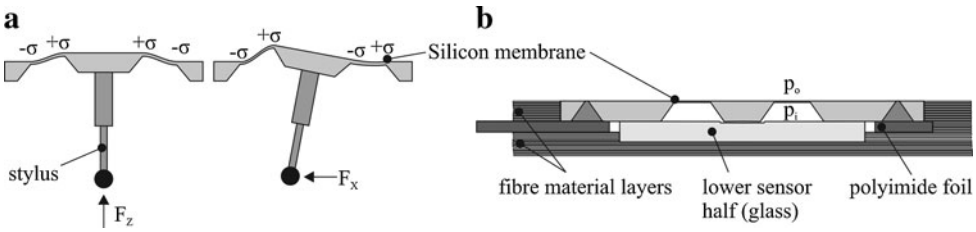

Fig. 2 Comparison between 3-D micro force sensor (**a**) and the new concept of tailor-made pressure sensor embedded in fibre material (**b**)

view of a 3D micro force sensor. Its characteristics have been published by Phataralaoha and Büttgenbach (2005) and were the basis of the investigations. In the first step, a new membrane shape which was adapted to the mechanical conditions (see "Simulation") was designed. The outer dimensions were then derived. Figure 2b shows the basic pressure sensor geometry. The minimum dimensions are defined by the limitations of micro fabrication and by the maximum possible accuracy. The micro fabricated parts include the silicon pressure sensor and the glass cover. The wiring is made of polyimide (PI) foil covered with a copper layer which was structured in house using a process similar to that for standard printed circuit boards (PCBs).

2.2 State of the art

Based on literature research, the sensor presented is the first embedded into fibre material. The unique advantages of the extremely flush mounting in the wall offer many new possibilities.

Until now, most sensors have components which are exposed to the streaming fluid and are therefore intrusive. Often a variety of surface fences or hot-wires (von Papen et al. 2004; Ebefors et al. 1998; Buder et al. 2007) are used as the sensing element in the flow. As well as having the disadvantage of changing the flow, these components are very fragile and susceptible to damage from particles in the flow. These sensors are therefore only applied for scientific measurements in the laboratories and also not likely suited for measurements in water.

The flush mounting of the sensor in the wall is a very important aspect of this sensor. Until now, many institutions have tried to design small sensors, which were later integrated into a model. The electrical connections were mostly placed downstream. In these cases, the sensor is placed flush within the wall, but the wiring not, as shown in the work of von Papen et al. (2004). In this new approach presented here, the integration of the sensors and the necessary subsystems directly into the wall is investigated. This is a necessary step in order to be able to control the state of the flow. In other micro-fabricated sensor projects, the creation of rounded contours was attempted. Very small pressure sensors were designed and fabricated. In order to better represent a perfect curved geometry many small sensors were placed in close proximity to each other. This reduces the radius of curvature and allows smoother flow.

Flexible sensors based on flexible substrates have been the topic in many recent publications (e.g. Buder et al. 2007). Hot-film sensors (e.g. by Tao of Systems Integration, Inc.) and pressure sensors have also been developed and are commercially available, but in very varying approaches.

In this approach, sensors are custom-made to be embedded into fibre composite material. This embedding process has extremely high demands on the sensor's capabilities, as illustrated in the following subsection. Since the embedding process is also being adapted for the integration of sensors, the concept seems to be feasible. Preliminary experiments with sensor dummies have been carried out by Beutel et al. (2010a, b).

2.3 Embedding into fibre material

Before the embedding process, the sensor with the wiring is positioned in several layers of composite material. Because the sensor is much thicker than a single layer of composite material, each layer has areas which are cut to fit perfectly around the sensor. Figure 2b shows a sectional view of the stack, which is mounted bottom up. The first fibre layers are uniform. Successive layers are cut out at the future sensor positions and layered to enable the placement of the glass part of the sensor. The sensor is then mounted together with the wiring. Finally the last layer, which is cut to the shape of the silicon part of the sensor, is added. This step is the most critical, because the overall height has to fit perfectly to the sensors. The actuators can be mounted in the same way.

In the laminating process, a protective cover has to be placed above and below the stack. This cover has a special finish to prevent sticking. After placing the stack in an autoclave, a pressure of 0.3 mbar is drawn between the two protection layers so that no gas remains. A pressure of 3 bar is then applied outside the protection layer before the preheated resin is pressed with 2.8 bar from one side to the other through the stack at 70°C. When all the resin is within the autoclave the in- and out-flow is closed properly for the 12 h baking process at 120°C. After opening the autoclave and removing the protection layers the laminating process is finished.

During this process, the sensors are exposed to high mechanical and thermal loads. Additionally the duration of the process is a critical factor. The sensors are designed to withstand these loads, and in the initial experiments they were able to resist the process. Currently, no sensor has been electrically tested after the embedding process. During the preliminary tests, either the sensors were dummies, or the wiring was not included. But by optical inspection it was found, that the membranes were not destroyed during the embedding process, showing that the micro fabricated sensors are suitable for the application. Since the lamination process itself is part of the research the first focus was on creating a planar surface, which has been successfully demonstrated.

2.4 Simulation of the membrane

The most crucial part of the doped silicon based sensor is the positioning of the piezoresistors on the diaphragm. The

design of the membrane itself has a large impact on the maximum loads, the size and the measuring aspects, e.g. linearity and resolution. Much effort is therefore necessary to develop a design, which has the desired properties and which is producible. In micro fabrication the limitations are given by the technologies which are available and by the type of wafer used.

As a starting point for design iteration, the force sensor shown in Fig. 2a was used. Because of the high pressures that must be measured (up to 4 bar), the area of the diaphragm has to be reduced, or the thickness has to be increased. Both changes reduce the mechanical stress on the diaphragm. In order to stabilize the diaphragm, a boss structure is recommended. During the embedding process, it acts as a mechanical limiter for the maximum deflection of the membrane. Figure 3a shows the geometry of the photolithographic mask used to structure the masking layers (silicon nitride and silicon oxide) on the wafer. At the white area the masking layers are removed in order to enable silicon wet etching in potassium hydroxide. The black areas are covered, avoiding any etching at these regions. The size of the compensation structures (X-structure in the center), which are necessary for anisotropic etching of (100)-silicon, leads to a minimum size of the membrane. Because the geometry of the membrane and the boss has a high impact on the sensor's behaviour, a simulation tool has been used. This tool (SUZANA) simulates the 3D wet etching process of silicon and was presented by Triltsch and Büttgenbach (2008). Hereby the final geometry can be visualized. Figure 3b shows the result of the simulation of the etching process for the sensor and the mask layout used for a wafer thickness of 360 µm. With the result of this simulation, which is the exact sensor geometry, the mechanical properties can be simulated using CosmosWorks®.

To determine the thickness of the membrane, all boundary conditions, and the safety factor adjusted maximum pressure have to be implemented in the FEM simulation. Because of symmetry effects, only one quarter of the sensor needs to be simulated. This reduces the simulation time significantly. In this way it is possible to find an optimum thickness for the membrane.

The results of this simulation are shown in Fig. 4. In Fig. 4a the deflection U_{RES} is given, while the mechanical stresses on the surface are shown in Fig. 4b. The quantitative

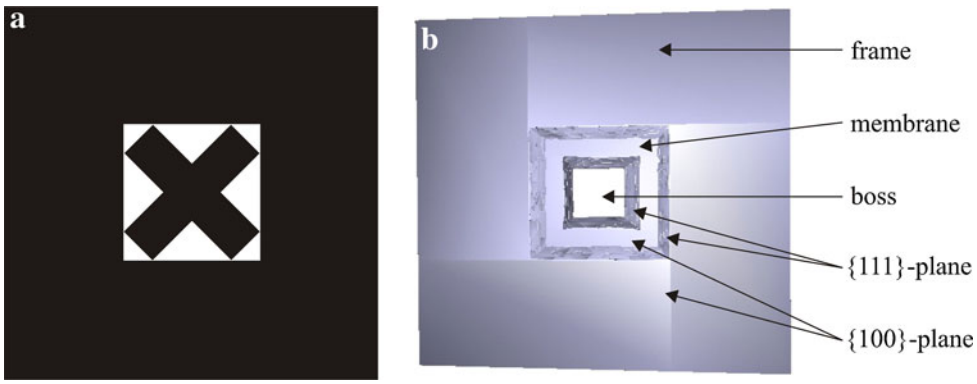

Fig. 3 Mask layout **a** used for the wet-etching process leading to the result shown in the *screenshot* **b** of the software tool SUZANA

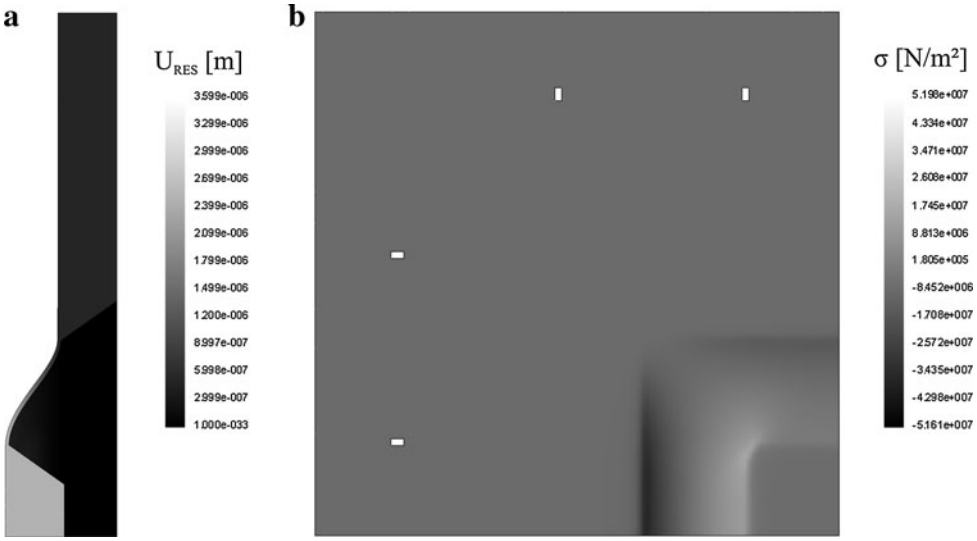

Fig. 4 Simulation results of CosmosWorks® **a** shows the deflection of the membrane, while **b** indicates the mechanical stress

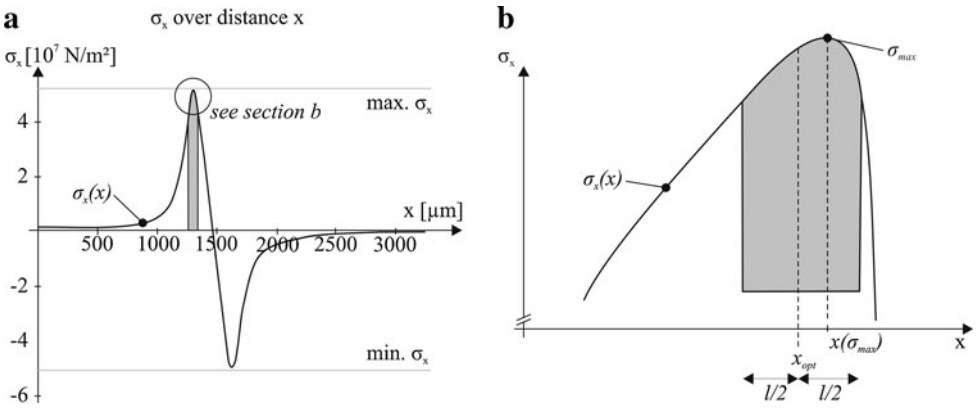

Fig. 5 The results of the simulation are shown in **a** above for the half sensor. A detailed view including the description of l and $x_{opt,\sigma max}$ is presented in **(b)**

values of the stress are exported into an Excel© sheet in order to compute the optimum position of the piezoresistors on the membrane. As described before, this influences the accuracy significantly. In Fig. 5a a plot of the numerical results is shown. The function $\sigma_x(x)$ shows the mechanical stress (N/m^2) depending on the distance x to the centre of the membrane. In order to get a high sensitivity of the sensor, the piezoresistors have to be placed at the locations of high mechanical stress to obtain a high ΔR. The analytical expression for the change of the resistance is given by

$$\frac{\Delta R}{R} = \pi_L \sigma_L + \pi_T \sigma_T \tag{1}$$

where σ represents the mechanical stress in lateral (index L) or transversal (index T) direction to the current. π is the piezoresistive coefficient depending on the doping process and the wafer material and orientation. This cannot be manipulated during the design process.

As the geometry of the piezoresistors has been optimized in the past, the length l has been fixed at 200 µm, leading to a constant value of R. As shown in Fig. 5a the mechanical stress σ is not constant. To find the optimal position for the center of the resistors, the average stress over the length has to be maximised. The mathematical expression can be described as follows:

$$x_{opt} = \left(\int_{x-\frac{1}{2}l}^{x+\frac{1}{2}l} \sigma(x)\mathrm{d}x \right)_{\max} \tag{2}$$

In Fig. 5a and b the area of integration is represented, where the integral reaches its maximum. Hence, x_{opt} is at the center of this span. According to Fig. 5b this position differs from the position of the maximum of $\sigma(x)$, what is an essential finding.

The simulation results are only valid for the maximum pressure difference between p_i and p_0 of 4 bar. They decrease if the pressure difference decreases. It has been demonstrated in Beutel et al. (2010a), that the values are also valid for a pressure difference of −4 bar, because the sensors' behaviour is reversible. The result of this simulation is an optimized membrane thickness of 45 µm and the value $\sigma_{max} \approx 5.5 \times 10^7$ N/m^2. Also the feasibility of the wet-eching process has been proved and the sensitivity S can be roughly determined.

$$S = \frac{\Delta U_0}{U_i}\frac{1}{p_0} \approx \frac{\sigma(x_{opt}) \cdot \pi}{p_{\max}}\frac{1}{U_i \cdot p_0} \approx 2.75\frac{mV}{V \cdot bar} \tag{3}$$

Thereby the average value for π, which is known from measurements in the past, and $\sigma(x_{opt})$ were used. In practice the sensitivity is much lower, because the physically true $\sigma(x_{opt})$-value is reduced due to the fact that it equals the average value of σ within the grey area of Fig. 5b which is in fact lower then σ_{max}.

3 Sensor fabrication

3.1 Standard fabrication process

The following fabrication process has been developed in order to realize the simulated design. The sensor has been fabricated on 4″ Si wafers in a batch process using state of the art technologies. The feasibility has been proved by several tests, in which various steps were completed independently. The first sensors were produced using steps 1–9, while the through–wafer connection was checked using steps 6–11 as described in Leester-Schädel et al. (2009). Figure 6 shows a simplified scheme of the most significant states during the process.

First, the diffusion of boron into the silicon substrate was used to fabricate the piezoresistors. For good ohmic contact, a highly doped "P+" area was added (2). Next, a Si_3N_4 layer is added as an etch stop layer for the through-wafer connections (3) before a SiO_2 is applied for electrical insulation (4). On the bottom side of the wafer, a SiO_2 and a Si_3N_4 layer were also deposited (5) to act as a second masking layer for wet-etching. The first masking layer was then structured (6) in order to allow advanced etching of

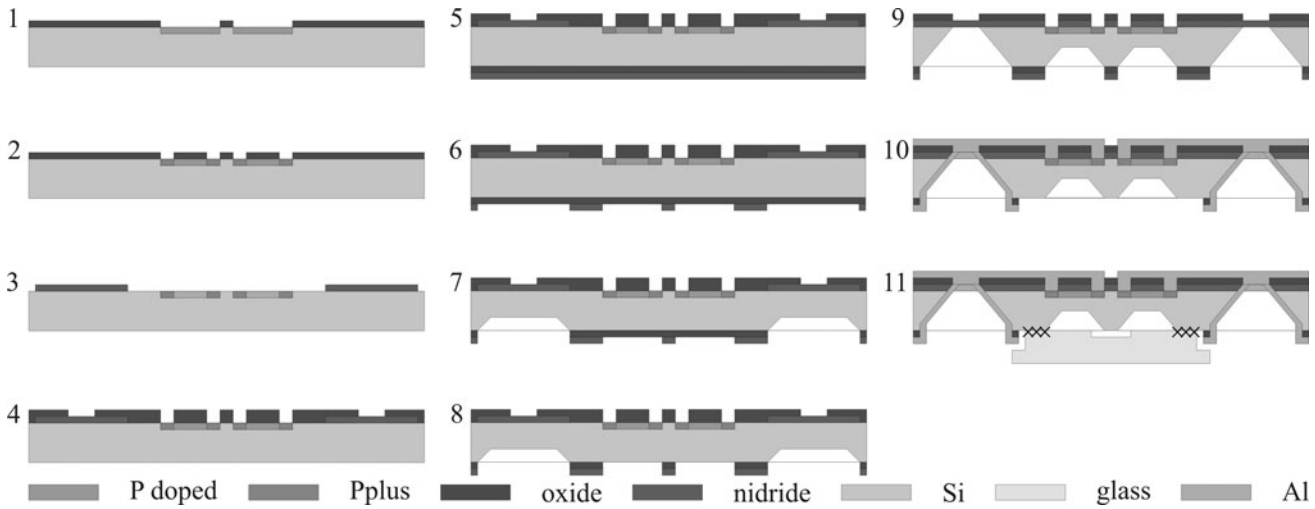

Fig. 6 Most significant process steps including bonding (not in scale)

45 µm at the connection positions (7). The second masking layer is then structured (8) so that in the second etching step for the membrane and the connections are etched simultaneously (9) until the membrane reaches the desired thickness and the wafer is through-etched, establishing the connections. After sputtering aluminum on the top side, the nitride is removed through dry-etching and the bottom side was sputtered with aluminum, so that an electrical connection could be generated (10). The aluminum was then structured on the bottom side and the oxide and nitride layers were removed to enable anodic bonding.

The glass cover was fabricated in a separate process. Here the glass is covered by a structured gold layer. The glass was then etched by a hydrofluoric acid solution. After the bonding process the wafers were diced, as explained in the "Improvements".

In the last step the sensor is fixed on the polyimide foil. Here a conductive adhesive, soldering paste or balls of solder can be used to fix the sensor and guarantee the electrical connection as well. Some experiments have been conducted and are continually being used to improve the pass rate.

3.2 Improvements

In this section, the latest improvements towards the future goal of a robust high precision sensor are described. The main focus is on the pressure cavity under the membrane and the anodic bonding of the lower sensor half (Fig. 2). Up to now, these glass covers have been glued manually piece by piece, because anodic bonding was not possible due to the through wafer connection. Also the high process temperature was thought to be problematic, because the pressure within the cavity under the membrane has a high impact on the range of p_0. Therefore, several techniques were used to enable a free settable value p_i. This could increase the range and accuracy of the sensors. For fabrication issues a batch process is desired, which leads to anodic bonding.

For anodic bonding of silicon and glass an anodic bonder is used. The two wafers, which have been aligned properly to each other in advance, are placed within this machine. The chamber is then heated to temperatures in the range of 300–500°C. A high DC potential of 50–1000 V has to be applied with an anode pressed on the top substrate to start the bonding process. Due to the electrical field and the elevated temperature a solid chemical bond between the substrates is created which is not reversible. To enable the process, both substrates have to be in contact. No other layers, such as metals, silicon oxide or nitride may be at the positions where the substrates have to be bonded. The fabrication process had to be improved for both parts: the sensor wafer and the glass wafer. The results are shown in Fig. 7.

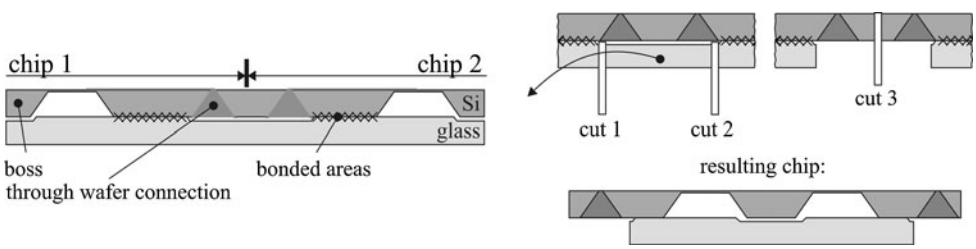

Fig. 7 **a** Drawing of the contact area between silicon and glass wafer, **b** cutting steps needed for production

The glass wafer is etched 4 µm at all positions where the silicon wafer has an overlap (see Fig. 7). By cutting the wafers in a special order from bottom side, the chips obtain the desired contour. In this way, the required time and effort for the assembly is reduced significantly.

The bonding parameters were set to $T_1 = 400°C$, $V = 400$ V and $p_1 = p_{ambient}$ for 2 h. The high process temperature leads to undesired properties in the sensor, since the cavity is closed at high temperature. Following the ideal gas law (Eq. 4) a bonding process at ambient pressure p_1 and $T_1 = 673.15$ K leads to a pressure within the cavity of $p_2 = 0.44$ bar after cooling down the chip to ambient temperature T_2.

$$pV = nRT \Rightarrow \frac{p}{T} = \frac{nR}{V} = const. \Rightarrow \frac{p_1}{p_2} = \frac{T_1}{T_2} \tag{4}$$

To avoid this reduced cavity pressure p_2 there are in principle three possibilities:

1. Decreasing temperature T_1 during bonding
2. Increase pressure p_1 during bonding
3. Implement channels for pressure balancing after bonding

The first possibility is not feasible, because a temperature reduction leads to poor bonding results.

For the second possibility, a pressure of 2.32 bar would be needed for compensation, which is technically not allowed in the bonder, because it exceeds the operation limit of the bonding machine.

Due to these limitations, the third solution seemed to be fruitful. Therefore, different channels were designed, shown in Fig. 8a–d. After bonding and cutting the wafers, the 8 µm deep channels were filled with SU-8 50 photoresist in order to close the cavity at room temperature. This negative resist was chosen because it has a high viscosity so it does not flow too deep into the cavity. The resist can be cured at 200°C so it is able to withstand the planned embedding process. The application of the resist was conducted manually with a dispenser (Fig. 8e). The resist then flows into the channel due to capillary action (Fig. 8f). After approximately 1 min the flowing process stops. Although this process proved to be very time intensive, it was demonstrated successfully. The resist also did not flow onto the membrane. The final position of the SU-8 is indicated in Fig. 8a–d by an arrow.

To reduce the time intensiveness, the above mentioned second solution was carried out in order to have a batch process. The anodic bonding machine was therefore carefully operated above its operating limits. The machine did not indicate any failures and the result was great.

Additionally to the adaption of the process plan, the creation of a cavity via anodic bonding was demonstrated. The pressure can be individually set up to 2.32 bar during the bonding process, leading to a customized pressure at ambient temperature in the cavity. Therefore, the range of the pressure sensor is raised, without any significant changes in the geometry or in the micro fabrication process.

4 Measurement results

For the first measurements with the custom made pressure sensors, a pressure chamber was designed. With this chamber automated tests are possible. It can be filled with water to simulate the real operating conditions mentioned in "Sensor concept".

The in-house air supply delivers dry and clean air at 8 bar. A precision proportional pressure regulating valve is used to control the pressure within the chamber. The valve has a 0–10 V input and delivers a voltage signal in the same range as output proportional to the pressure. Therefore, the actual pressure p_{actual} indicated by the valve can be measured. The valve has a maximum accuracy of ±50 mbar within the range of 0–6 bar, according to the manufacturers' information. A 16-bit DAQ System is used to control the valve as well as its sensor. At the connector block, five analog inputs are used to convert the output voltages of the four amplified sensor bridges and the valves' sensor. One analog output is used to provide the input voltage of the valve.

Inside the chamber the micro-fabricated sensor is connected to a feedthrough, which is plugged into a four channel signal amplifier. Furthermore the amplified sensors' signals are fed to four other analog inputs of the DAQ system. Figure 9 shows the simplified system set-up.

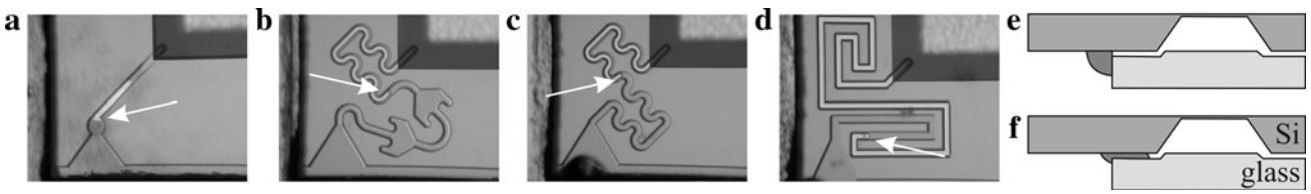

Fig. 8 **a–d** *Four* photos of different channel types leading into the cavity, **e**, **f** show principle of the sealing process

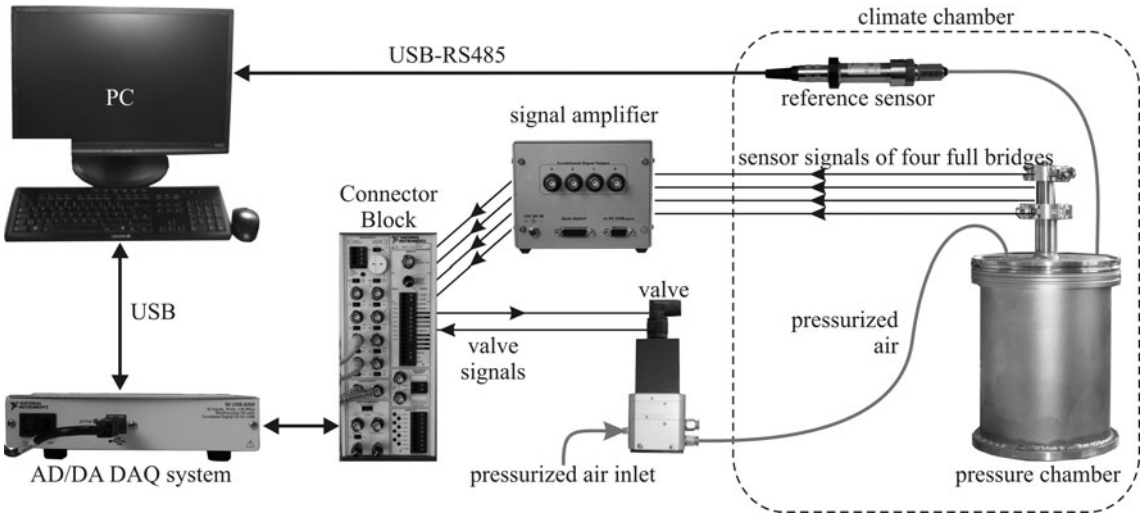

Fig. 9 Simplified set-up of the calibration system including the climate chamber

All measurements have been taken using this setup. The system currently operates at pressures up to 1.5 bar, which is the maximum approved pressure range of the feedthroughs and the pressure chamber. For future experiments, feedthroughs which are suitable for pressures up to 4 bar, are necessary to improve the performance and to enlarge the measurable pressure range.

In this section the set-up and the results of the preliminary tests are presented. The results show the repeatability and linearity of the sensor. In addition to the first measurements a comparison with a reference sensor is drawn to enable a comparison of the absolute accuracy.

4.1 Recalibration of the proportional valve

During the tests, the pressure in the chamber is altered stepwise using LabView® control software. The entire procedure is illustrated in Fig. 10. In the software, different test cycles have been programmed. Mostly a stepwise pressure change is used, where the maximum and the minimum pressure (p_{min}, p_{max}) can be regulated. Additionally, the amount of steps n and the stabilization time t_S can be adjusted. Due to the thin tubes and the relatively high volume of the chamber (ca. 8 l) it takes some time (<2 s) until the pressure in the chamber reaches the desired value given by the valve. After a short stabilization period the pressure becomes constant. The program then begins to acquire the sensor signals from the micro fabricated sensor V_{out} as well as the valves' pressure sensor p_{actual}. The step height p_S is calculated by the program using p_{max}, p_{min} and n. Directly after the measurement, the pressure is changed to the next value p_{given}, and the same routine at the new pressure step is performed.

During these tests we found out, that the pressure in the chamber is constantly lower than the desired value p_{given}, what is caused by the valve. Additionally we figured out, that the valve's sensor is more precise than the valve itself. A reference sensor (0.01% accuracy full scale) which has been installed verified this assumption. This motivated us to develop a simple correction algorithm in order to achieve pressures within the chamber more close to the desired pressure.

Figure 11 shows the difference between the valves' sensor signal p_{actual} and the desired value p_{given} over the actual pressure p_{actual}. An offset as well as a slope of the averaged data are obvious.

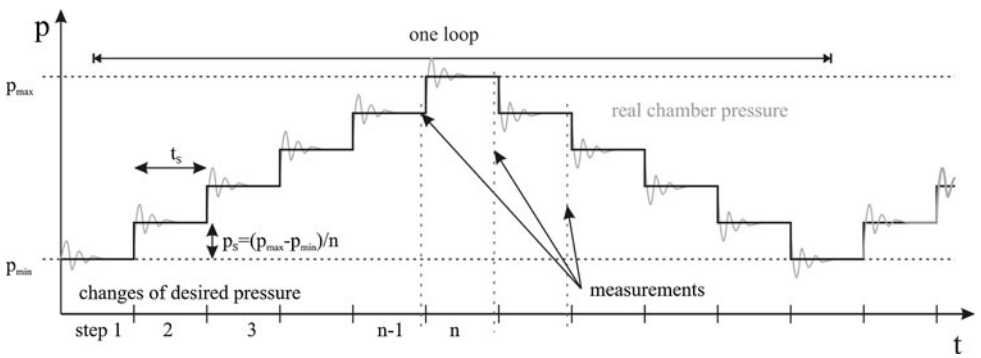

Fig. 10 Illustration of the timeline indicating the real pressure p above time t and the steps automatically controlled by the LabView routine

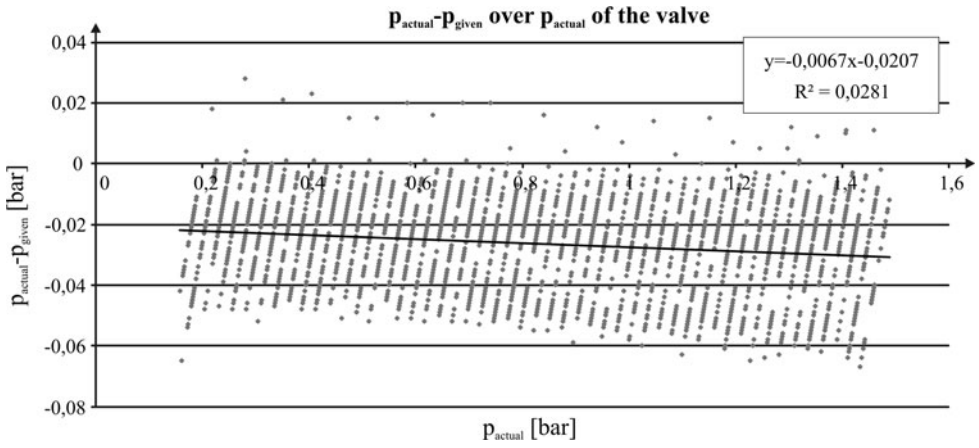

Fig. 11 Valves' sensor signal p_{actual} minus the given pressure p_{given} over given pressure including a linear regression curve with its formula

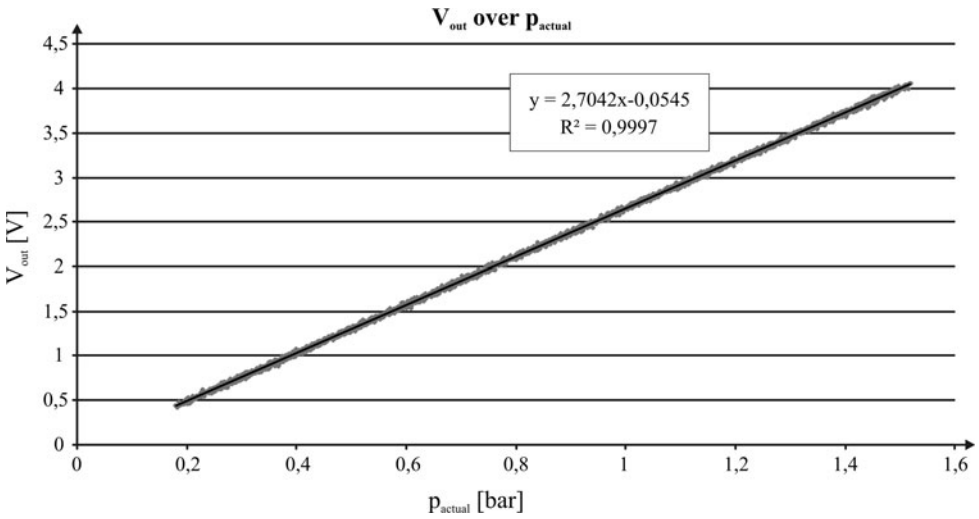

Fig. 12 Signals from micro fabricated sensor (*bridge 1*) V_{out} over corrected actual pressure $p_{actual,corr}$

For the measurements with our sensor we fitted the output voltage to the valve using the linear regression formula given in Fig. 11 to get the pressure in the chamber closer to the desired pressure. In fact, it is not possible to raise the accuracy by doing so, this solution just minimises the systematic errors introduced by the valve.

The manufacturer of the valve indicates the maximum accuracy of ±50 mbar. As one can see, the discrepancy is sometimes higher than this value. After the correction with the formula, only two of 3,000 measurement points are outside this range, and the linear average is 0.

$$p_{actual,corr} = p_{actual} + 0.0067 \cdot p_{actual} + 0.0207 \;\; bar \qquad (5)$$

4.2 Linearity of the sensor

Another intention during the development was to create a sensor with a linear behaviour. Although the tests were performed in the range of 0–1.5 bar, and not until the absolute design limit, the results are promising.

Figure 12 shows the amplified sensor signals over the actual pressure. The formula given in the diagram is the transfer function. It does not represent the real output of the sensor, because an operational amplifier is used. Therefore, the slope has to be divided by the amplification factor and the supply voltage. The offset has also been cancelled out by the signal conditioner. Anyhow, the system can be calibrated using the curve and the linear behaviour is evident.

Figure 13 indicates the difference between a linear regression of the pressure signal $p_{out,lin}$ and the actual pressure value p_{out} over the corrected pressure $p_{actual,corr}$. The deviations are well distributed. Using a linear regression for the deviations nearly no slope (3×10^{-12} mbar/bar) is detectable. Also for polynomial fittings of the 2nd or 4th order the parameters are in a very small magnitude.

In the current range, the maximum residuals of about ±20 mbar comply with a output voltage of 0.05 V. Measuring a linear behaviour of our sensor at a pressure range of 0–1.5 bar, it can be assumed that the linearity remains constant until a pressure of 4 bar.

4.3 Time capability

The eigenfrequency of the fabricated sensor has been simulated with CosmosWorks© and was calculated to be

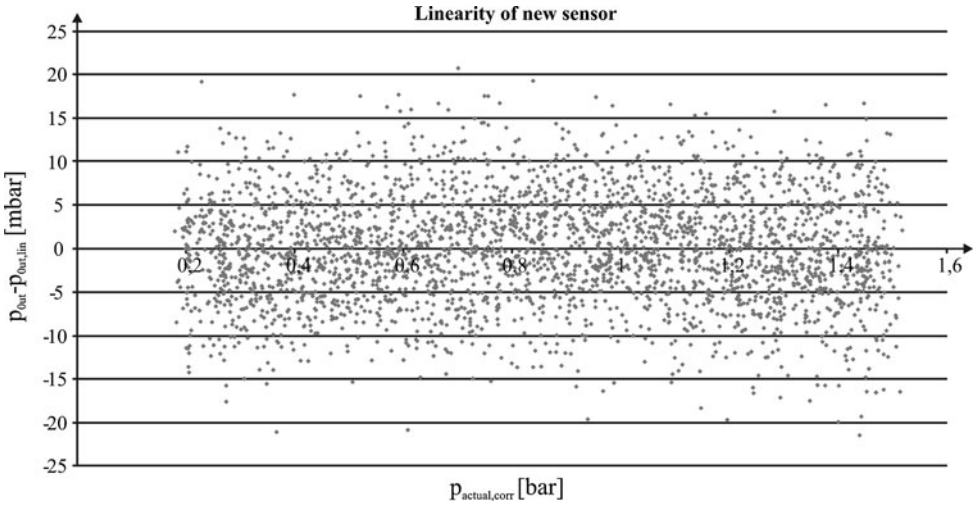

Fig. 13 The difference of p_{out} and the linear regression $p_{out,lin}$ from micro fabricated sensor (*bridge 1*) over $p_{actual,corr}$

between 9.46×10^9 (=1.51×10^9 Hz) and 9.08×10^9 rad/s (=1.44×10^9 Hz). This frequency is very high compared to other sensors. As shown in Fig. 3b the boss occupies a large area of the membrane. Therefore, the deformable area is quite small. Taking into account, that the membrane has to withstand a high pressure difference, it has to have a relatively high thickness. These geometric effects lead to a stiff membrane with a high eigenfrequency. The boss' mass, intented to lead to a lower eigenfrequency, does not negotiate the effect of the membrane stiffness.

Up to now, there is no motivation to test this eigenfrequency, because this frequency is 4×10^3 times higher than the measuring frequency, which is limited by the amplifier and the DAQ system. The amplifier used has a bandwidth (−3 dB) of 300 kHz per channel and the DAQ system has a sampling rate of 1 MS/s at 16-bit mode using more than one channel. Whether the amplifier or the DAQ system is the limiting component depends on the amount of channels used simultaneously. One DAQ system can handle three amplifier modules of that type. When using more, the DAQ system is the limiting factor. Tests are scheduled to find qualified values for the noise and temperature effects.

5 Conclusions and outlook

The initial measurements with the newly installed set-up fulfilled all expectations. The entire design and development process has resulted in a very linear and robust pressure sensor.

In the near future, steps will be taken to verify the sensors' sensitivity and the correct position of the piezoresistors. For comparison reasons, all measurements have been performed with the same sensor. In order to determine the value deviation from sensor to sensor coming from the same wafer, other sensors have to be measured. A comparison between the theoretical maximum sensitivity S given in (Eq. 3) and the measured sensitivity could then be maintained.

To increase the overall accuracy of the sensors, the temperature within the chamber has to be controlled. Due to the pressurized air, which might cool the inside of the chamber during expansion, some temperature effects may have an influence on the sensor. As an indication for this effect, we found a dependency between the temperature and pressure values of the reference sensor. High pressures have constantly been read out at relatively high temperatures, while the lower reference pressures have been read out at lower temperatures. This leads to the assumption, that during pressure increase phase from p_{min} to p_{max}, temperature decreases (ca. 0.1 K). A temperature sensor in the pressure chamber might give detailed explanations. Additionally, the pressure chamber including the reference sensor could be placed in a climate chamber (see Fig. 9) to avoid temperature drift caused by day/night changes. Also temperature compensation of the output signal can be performed by doing so.

With new equipment, the pressure range of the chamber has to be increased to the desired maximum pressure in order to enable measurements of the full span. To improve the electrical contact new connectors from the inner to the outer of the pressure chamber will be used to improve the signals' quality. The wiring itself will be shortened and better shielded wires will be used.

Aside from the pressure sensor itself, related issues such as embedding working sensors with all implemented features into the fibre material have to be performed. Thereafter new tests are required to check if the embedding process has any influence on the sensors behaviour. In the future, a hot-wire anemometer will be integrated on the chip of the pressure sensor.

Acknowledgments This work was funded by the German Research Foundation in the framework of the collaborative research centre 880 "Fundamentals of High Lift for Future Civil Aircraft".

References

Berns A, Buder U, Wang X. H, Nitsche W, Obermeier E (2008) AeroMEMS pressure sensor with integrated wall hot-wire. In: Proceedings of the IEEE Sensors. doi:10.1109/ICSENS.2008.4716746

Beutel T, Ferreira N, Balck A, Leester-Schädel M and Büttgenbach S (2010a) Cell manipulation system based on a silicon micro force sensor with self-calibration from backside. In: Proceedings of the IEEE sensors. doi:10.1109/ICSENS.2010.5690506

Beutel T, Leester-Schädel M, Wierach P, Sinapius M, Büttgenbach S (2010b) Novel pressure sensor for aerospace purposes. IFSA Sens Transducers J 115:11–19 ISSN 1726-5479

Buder U, Henning L, Neumann A, Obermeier E (2007) Aeromems Wall hot-wire sensor arrays on polyimide with through foil vias and bottom side electrical contacts. In: Proceedings of transducers 2007, p 3E02. doi: 10.1109/SENSOR.2007.4300637

Ebefors T, Kälvesten E, Stemme G (1998) Three dimensional silicon triple-hot-wire anemometer based on polyimide joints. In: Proceedings of the eleventh annual international workshop on micro electro mechanical system: an investigation of micro structures, sensor, actuators, machines and systems, Heidelberg, 25–29 January 1998, pp 93–98

Leester-Schädel M, Beutel T, Büttgenbach S (2009) Entwicklung eines Herstellverfahrens fuer die rueckseitige, elektrische Kontaktierung von mikrotechnischen Membransensorelementen. In: Proceedings of MST Kongress, Berlin 2009, pp 746–749

Phataralaoha A, Büttgenbach S (2005) A novel design and characterization of a micro probe based on a silicon membrane for dimensional metrology. In: Proceedings of Eurosensors XIX, Barcelona, 2005, p WPb31

Schiffer M, Obermeier E, Grewe F, Ebner A, Fernholz H (2005) A new height-adjustable aeroMEMS surface fence probe fabricated in SOI technology for high resolution wall shear stress measurement in turbulent flows. Transducers 2005, Digest of Technical Papers, pp 601–604

Triltsch U, Büttgenbach S (2008) Next Generation of TCAD Environments for MEMS Design. In: Proceedings of the symposium on DTIP of MEMS/MOEMS. doi:10.1109/DTIP.2008.4752959

von Papen T, Buder U, Ngo H, Obermeier E (2004) A second generation MEMS surface fence sensor for high resolution wall shear stress measurement. Sens Actuators A 113:151–155. doi:10.1016/j.sna.2004.01.058